

CHEMISTRY

A European Journal

A Journal of



Accepted Article

Title: Imprinted naked Pt nanoparticles on N-doped carbon supports: A synergistic effect between catalyst and support

Authors: Jairton Dupont, Gustavo R. Bolzan, Gabriel Abarca, Wellington D. G. Gonçalves, Carolona F. Matos, and Marcos J. L. Santos

This manuscript has been accepted after peer review and appears as an Accepted Article online prior to editing, proofing, and formal publication of the final Version of Record (VoR). This work is currently citable by using the Digital Object Identifier (DOI) given below. The VoR will be published online in Early View as soon as possible and may be different to this Accepted Article as a result of editing. Readers should obtain the VoR from the journal website shown below when it is published to ensure accuracy of information. The authors are responsible for the content of this Accepted Article.

To be cited as: *Chem. Eur. J.* 10.1002/chem.201704094

Link to VoR: <http://dx.doi.org/10.1002/chem.201704094>

Supported by
ACES

WILEY-VCH

Imprinted naked Pt nanoparticles on N-doped carbon supports: A synergistic effect between catalyst and support

Gustavo R. Bolzan,^[a] Gabriel Abarca,^[a] Wellington D. G. Gonçalves,^[a] Carolina F. Matos,^[b] Marcos J. L. Santos^[a] and Jairton Dupont^{*[a]}

Abstract: A synergistic effect resulting from the interaction of small (2.4–3.1 nm) naked Pt nanoparticles (NPs) imprinted on N-doped carbon supports is evidenced by structural, electronic and electrochemical characterization. The size and distribution of the sputtered Pt NPs are found to be related to the nature of the support, as Pt NPs are preferentially located at N_{graphitic} sites. In addition, Rutherford backscattering shows that a deeper penetration of the Pt NPs is obtained in the N-doped carbon support with larger pore diameters. The ligand effect of the N-doped carbon supports is found to occur by electron donation from N_{pyrrolic} and N_{graphitic} sites to the Pt NPs and the electron acceptor behaviour of the C=N_{pyridinic} sites. The carbon matrix acquires a basic characteristic (electron-richer, metallic behaviour) capable of interacting with metallic NPs akin to a bimetallic-like system. The imprinted Pt NPs are active catalysts for oxidation, while displaying poor catalytic activity for reduction reactions. The catalyst N-doped carbon supports play an important role in the overall catalytic process, rather than only acting as a simple active phase carrier.

Introduction

Carbon and graphite nanostructures present unique physical and chemical properties, such as high electrical conductivity^[1,2], chemical stability,^[3] high surface areas and porosity.^[4] The combination of these properties makes this class of material very interesting for a wide range of applications, including gas sorption^[5] and separation,^[6] energy conversion,^[7] energy storage^[8] and as catalyst supports.^[3,9,10] Among all of the investigated applications, the combined characteristics of a large surface area with high electrical conductivity mean that these carbon-based materials are widely applied as catalyst and electro-catalyst supports.^[11] Although, carbon-supported Pt nanoparticles (NPs) are certainly one of the most investigated catalytic systems,^[12–14] their low stability is still a main drawback towards the widespread application of these materials.^[3,12,15] To obtain efficient, yet stable carbon-supported Pt NP catalysts,

tremendous effort has been made to develop state-of-the-art nanohybrid materials.^[15,16] The commonly used synthetic approaches involve complex processes for Pt encapsulation or adsorption at the nanocarbon surface and are carried out using, for example, expensive porous inorganic host materials.^[17] On this basis, sputtering deposition can be considered a powerful technique that allows for fine control of the NP size by simply controlling the current discharge and metal concentration during deposition.^[18,19] In addition, no by-products are generated using this technique. The obtained catalytic material is only composed of well-dispersed NPs and the carbon support, thus allowing for a more accurate analysis of the carbon support-Pt NP interface.^[20] As previously shown in the literature, by doping carbon with nitrogen, one can tune the electrical conductivity, basicity, oxidation stability and catalytic activity of the support.^[2,21–23] Additionally, the presence of the nitrogen heteroatom in N-doped carbon (CNd) not only allows for the maintenance of the catalytic phase in a well dispersed state, but also affects the catalytic activity, either by direct participation in the reaction mechanism or by favouring the interactions between the active phase and support.^[24] These supports present the desired properties of a catalyst, such as inertness towards unwanted reactions, stability under regeneration and reaction conditions, adequate mechanical properties, tunable surface area, porosity.^[24–26]

We demonstrate the application of sputtering deposition for the generation of well-distributed naked Pt NPs on CNd supports. It is explored the combined effect of nanoscale confinement and the CNd support on the catalytic and electrocatalytic properties of the imprinted naked Pt NPs. The effect of the support on the Pt NP properties are rationalised by considering the interaction between the N-containing ligands (Lewis acid/bases) and the naked Pt NP.

Results and Discussion

Preparation and characterisation of Pt-NPs imprinted on CNd supports.

CNd supports were prepared using a well-established nanosilica template method^[27] employing ionic liquids (ILs). The obtained CNd supports were labelled as **CN0** obtained from 1-butyl-3-methylimidazolium dicyanamide [BMIm][dca], **CN1** from 1-butyl-3-methylimidazolium dicyanamide [BMIm][dca] and **CN2** from 1,3-bis(butyl-3-methylimidazolium dicyanamide [DBCNIm][dca], respectively ILs **1–3** (Table 1). The concentration of N in the CNd supports was controlled by the stoichiometry of the chosen IL (for details see SI, Table S1).^[28–30] The blue shift of the G-band position in the Raman spectra along

[a] Institute of Chemistry
Universidade Federal do Rio Grande do Sul - UFRGS
Av. Bento Gonçalves, 9500, CEP 91501-970, Porto Alegre, RS,
Brazil.
E-mail jairton.dupont@ufrgs.br

[b] Universidade Federal do Pampa
Av. Pedro Anunciação 111, CEP 96570-000, Caçapava do Sul,
Brazil.

Supporting information for this article is available on the WWW
under <http://dx.doi.org/10.1002/chem.2017xxxxx>.

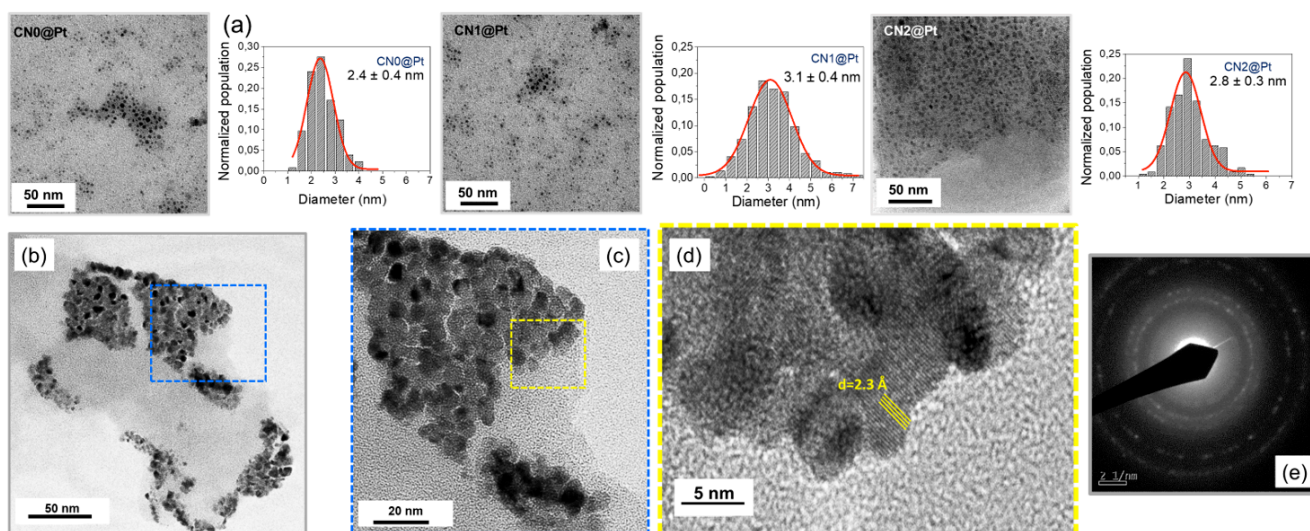


Figure 1. a) TEM micrographs and size distribution histograms of CN0@Pt, CN1@Pt and CN2@Pt catalysts and b), c) and d) HRTEM micrographs and (e) electron diffraction analysis of CN1@Pt.

with the larger concentration of nitrogen strongly indicates a decrease of the size of C sp^2 domains as a function of the nitrogen content (for details see SI, Figure S2).^[21]

Figure 1 shows the transmission electron microscopy (TEM) images from the CNd@Pt obtained by sputtering Pt NPs on the CNd supports. The Pt NPs in all the samples present an average diameter of ca. 2.8 nm, confirming the fine size control obtained by sputtering deposition. The HRTEM images (Figures 1b-d) show that the Pt NPs are equally distributed on the surface of the carbon support (for details see SI, Figures S3-S4). The interplanar distances of the crystal planes observed in Figure 1d were calculated based on electron diffraction (Figure 1e) and were found to be 2.3, 2.0, 1.3 and 1.2 Å for the (111), (200), (220) and (311), planes, respectively, indicating the formation of Pt in a cubic crystal system.^[31]

Table 1. Surface areas, pore diameters and carbon and nitrogen concentrations in the CNd (CNd %C %N) as a function of IL precursors 1–3.

| Entry | IL precursor | Sample | S_{BET} ($\text{m}^2 \cdot \text{g}^{-1}$) ^[a] | Pore diameter (nm) ^[b] | CNd ^[c] %C | %N |
|-------|--------------|--------|--|-----------------------------------|-----------------------|-------|
| 1 | 1 | CN0 | 318.7 | 4.11 | 77.56 | 11.91 |
| 2 | 2 | CN1 | 326.7 | 4.67 | 76.54 | 12.32 |
| 3 | 3 | CN2 | 158.5 | 4.71 | 77.68 | 15.02 |

[a] Specific surface areas were determined by the BET multipoint method. [b] Average pore sizes were obtained by the BJH method. [c] Determined by elemental analysis.

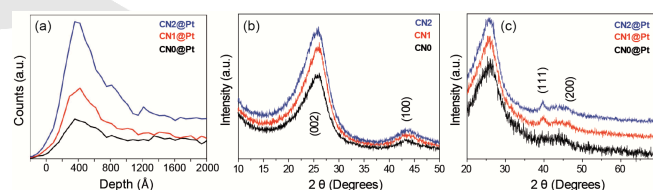


Figure 2. (a) Depth profile of Pt NPs on CNd@Pt catalysts determined by RBS, (b) XRD patterns of CNd catalyst supports and (c) XRD patterns of CNd@Pt materials.

Rutherford backscattering spectroscopy (RBS) was used to estimate the depth profile of the Pt NPs in the CNd supports (Figure 2a). It is possible to observe a relation between the Pt NP distribution with the pore diameter of the CNd. CN0, which presents the smallest average pore diameter (4.11 nm), exhibits the highest quantity of NPs at the superficial regions when compared to deeper regions. Alternatively, supports with larger pores, CN1 (4.67 nm) and CN2 (4.71 nm), present a broader depth profile, indicating easier penetration of the Pt NPs into the supports. X-ray diffraction (XRD) analysis of all the samples present diffraction patterns at ca. 25.25° and 43.80°, corresponding to (002) and (100) reflections from graphitic pore walls (Figure 2b).^[32,33] The intensity of the peak at 43.8° confirms the crystalline structure of the as-prepared CNd. The d spacing of the (002) peak is found at ~0.347 nm, which is slightly larger than from pristine graphite ($d = 0.335$ nm) and is similar than the d spacing from graphitic CNd materials.^[32,33] Hence, the presence of a turbostratic arrangement of carbon and nitrogen atoms in the CNd wall is quite probable. The XRD patterns of

the CNd@Pt (Figure 2c) present diffraction peaks related to the (111) Pt NPs plane at ca. 39° and (200) at ca. 46°. In fact, one cannot observe the (111) plane for CN0@Pt, probably due to the small amount of Pt NPs (see the XPS results). These data combined with those obtained by electron diffraction confirm the face-centred cubic system for Pt NPs (belonging to the space group Fm3m).^[34]

The Raman spectra of the CNds and CNd@Pt (Figure 3) show two main vibration modes in the 800–1800 cm⁻¹ region, the G band (~1570 cm⁻¹) and D band (~1320 cm⁻¹). Nitrogen atoms within a sp² carbon structure favour the formation of pentagons and hexagons (for details see SI, Figure S5), thereby increasing the reactivity of neighbouring carbon atoms, resulting in an increased degree of disorder within the CNd. This disorder was evaluated by the ratio intensity of the D and G bands (I_D/I_G).^[28] The results show a slight decrease of the I_D/I_G ratio from CN0 to CN1 and a significant increase for CN2 (for details see SI, Figure S2), indicating higher structural disorder in this sample. The effect of the Pt NPs on the structure of the support can also be observed by the increase of the I_D/I_G ratio and the shift of the D and G bands to larger wavenumbers. These changes are much probably related to direct interaction of the Pt NPs with the support (see below).

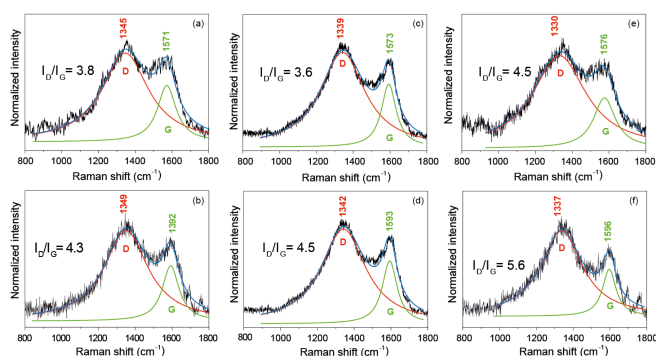


Figure 3. Fitted Raman (Lorentzian model) of CNd samples: (a) CN0, (b) CN0@Pt, (c) CN1, (d) CN1@Pt, (e) CN2 and (f) CN2@Pt, D and G band position in CNd samples.

The areas in percentage for each N-type present in the CNd@Pt nanocomposites were obtained from XPS and are described in Table 2. The N 1s region from the CNd was deconvoluted into five components related with different nitrogen types: $N_{\text{pyridinic}}$, N_{pyrrolic} , $N_{\text{graphitic}}$, N_{ox} (oxides N, NO₂) and N_{ads} (N adsorbed on the surface) (for details see SI, Figure S5). An important result is the predominant species on the CNd surfaces; graphitic > pyridinic > and pyrrolic, rather than the oxide species usually obtained from post-synthesis doping.^[15]

XPS analyses were performed to evaluate whether the CNd support could affect the electronic properties of the Pt NPs. The XPS spectra of the Pt 4f region are presented in Figure 4. All the CNd@Pt samples present Pt NPs in the reduced state (Pt(0)).

Table 2. Percentage of each nitrogen type found at the surface of CNd and CNd@Pt samples by deconvolution of the N 1s region in high-resolution XPS.

| Entry | Sample | $N_{\text{graphitic}}$ (%) | N_{pyrrolic} (%) | $N_{\text{pyridinic}}$ (%) | N_{ox} (%) | N_{ads} (%) |
|-------|--------|----------------------------|---------------------------|----------------------------|---------------------|----------------------|
| 1 | CN0 | 41.51 | 12.51 | 28.21 | 13.72 | 4.26 |
| 2 | CN1 | 38.87 | 16.16 | 29.04 | 9.99 | 5.94 |
| 3 | CN2 | 39.34 | 18.62 | 32.06 | 6.76 | 3.28 |
| 4 | CN0@Pt | 31.84 | 21.48 | 25.11 | 14.94 | 6.63 |
| 5 | CN1@Pt | 31.59 | 19.32 | 30.04 | 14.74 | 4.31 |
| 6 | CN2@Pt | 35.30 | 19.14 | 34.42 | 7.58 | 3.55 |

The Pt NPs deposited on carbon supports can present a slight shift of the Pt 4f spectrum to higher binding energies, due to a decrease in Pt particle size.^[35–37] Interestingly, in the present work, the XPS signals of Pt(0) are significantly shifted (0.5–0.7 eV for Pt 4f_{5/2} and 4f_{7/2}) for higher energies compared to bulk Pt (4f_{5/2} = 73.7 and 4f_{7/2} = 70.4 eV).^[38,39] In addition, this shift has also been found to indicate that the Pt atoms presents in the CNd@Pt are electron-richer than in bulk Pt and naked Pt NPs imprinted on oxides supports.^[40,41] Therefore, the CNd support clearly affects the electronic structure of the Pt NPs.

To understand how the support affects the electronic levels of the Pt NPs, the binding energies (BEs) from N 1s in all of the samples with and without Pt NPs (for details see SI, Table S6) were evaluated. For CN0 and CN2, the BE of the $N_{\text{pyridinic}}$ shifts to lower energies, indicating that C=N_{pyridinic} is acting as a Lewis acid. Alternatively, the BE of $N_{\text{graphitic}}$ and N_{pyrrolic} shift to higher energies, hence acting as Lewis bases. Another interesting observation is the significant decrease of the $N_{\text{graphitic}}$ percentage in the supports containing Pt NPs along with simultaneous increases in N_{pyrrolic} and $N_{\text{pyridinic}}$. This behaviour indicates that Pt NPs are preferentially located at the graphitic sites, which can be explained by the stronger electron donation on those graphitic sites, as previously observed by theoretical studies.^[42]

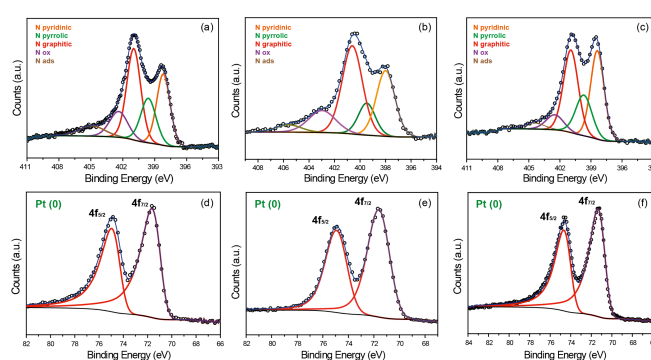


Figure 4. High-resolution XPS spectra (a-c) of N 1s for CN0@Pt, CN1@Pt and CN2@Pt and (d-f) Pt 4f regions respectively.

The XPS analysis presented in Table 2 corroborates the Raman data, showing that a higher percentage of pyrrolic and pyridinic nitrogen is present in CN2. The XPS analysis revealed the

presence of five nitrogenous compounds, hence the pyrrolic and pyridinic defects are mainly responsible for increasing the intensity and red shift of the D band in the Raman spectra (for details see SI, Figure S2 and S5).^[21]

Table 3. Binding energy (eV), FWHM and percentage of Pt NPs found at the surface of CNd@Pt samples by deconvolution of the Pt 4f region with high-resolution XPS.

| Entry | Sample | 4f _{5/2} (eV) | FWHM | 4f _{7/2} (eV) | FWHM | %Pt (XPS) |
|-------|--------|------------------------|------|------------------------|------|-----------|
| 1 | CN0@Pt | 74.48 | 1.57 | 71.15 | 1.55 | 0.33 |
| 2 | CN1@Pt | 74.55 | 1.95 | 71.23 | 1.91 | 1.70 |
| 3 | CN2@Pt | 74.21 | 1.52 | 70.88 | 1.52 | 1.43 |

Electrochemical properties

Figure 5 shows the cyclic voltammograms of all the samples together with a standard carbon black without Pt NPs (C0) and standard carbon black with Pt NPs (C0@Pt), which were used as backgrounds. As observed in Figure 5a, the cyclic voltammograms of C0, as well as CN0, CN1 and CN2, do not display hydrogen adsorption/desorption peaks, however in C0@Pt, CN0@Pt, CN1@Pt and CN2@Pt, the characteristic peaks are observed within 0–0.1 V. In addition, it is possible to observe that Pt oxidation is taking place in a wide potential range. The presence of a single anodic peak related to hydrogen desorption and a single cathodic peak related to hydrogen adsorption centred at ca. 0 V indicate that reactions are taking place over isolated Pt NPs rather than a Pt film.^[43]

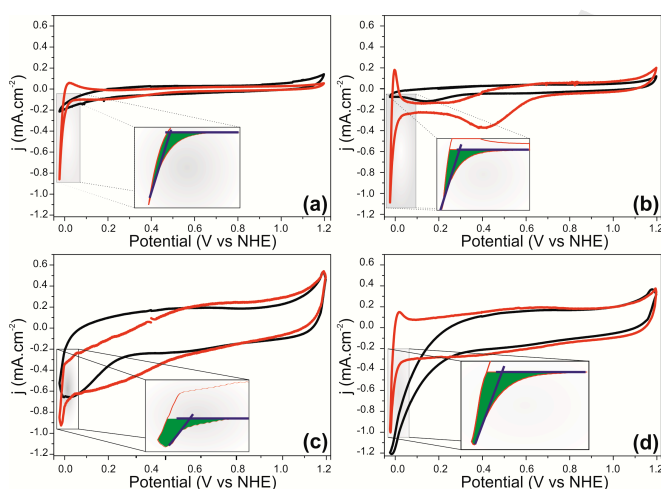


Figure 5. Cyclic voltammetry of CNd (black) and CNd with Pt NPs (red): a) C0, b) CN0, c) CN1 and d) CN2. Insets show the adsorption/evolution area (green) and onset potential (blue line) for hydrogen evolution.

Comparing the voltammograms obtained from the CNd, one can observe the increasing capacitive behaviour of the CNd supports when compared to C0 (Figure 6a). In addition, Figure 6a shows the values obtained from the difference between the cathodic and anodic current in the region of the double layer, located at 0.5 V. These data reflect the comparative effect of the accumulation of load capacity on the CNd materials. This

phenomenon is owed to the presence of nitrogen in the carbon matrix, resulting in a reinforcement of the π bonds that increases the capacity for forming a double layer at the electrode/interface.^[44]

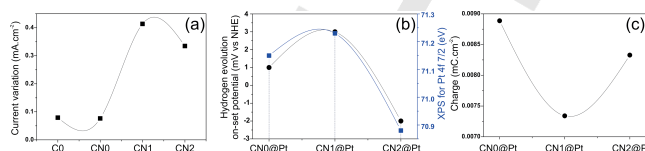


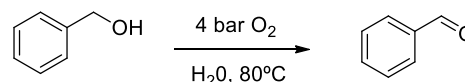
Figure 6. a) Current variation at 0.5 V relative to capacitive area in CNd without Pt-NPs. b) Variation of hydrogen evolution on-set potential (black spot) and comparison against BE to Pt 4f_{7/2} (blue square) of CNd@Pt. c) Charge of the hydrogen adsorption/evolution area. The plotted lines are a guide to the eyes.

The displacement of the potential on-set for hydrogen evolution^[45] (Figure 6b) shows the effect of the CNd supports interaction with the Pt NPs, affecting the energy necessary for the reduction of H⁺ species in solution. The observed variation of potential (1.8 mV, 3mV and -2mV for CN0@Pt, CN1@Pt and CN2@Pt, respectively) is owed to the synergistic effects of the interaction between a NP and the support, which reflects directly without potential in the onset of hydrogen evolution and in the BE obtained by XPS.^[46–48] This variation is also related to the energies associated with the Pt 4f_{7/2} orbital shown in Table 3.

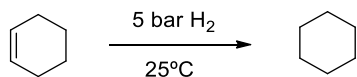
The area of the cathodic adsorption/evolution peak (ACAEP) obtained by integrating the potential cathodic peak near 0 V^[49,50] is larger for the CN0 than the hybrid materials (Figure 6c). The ACAEP directly reflects the interaction capacity of the NPs with H⁺ and H₂ species and its change is another indication of synergistic surface effects in CNd@Pt materials.^[51] In this case, the lower free Gibbs energy for the hydrogen adsorption is closest to zero and hence the adsorption of hydrogen species is more favourable in CN0 as compared to others CNd supports. The CNd supports display a basic character (electron-rich, metallic-like behaviour) and by interacting with metallic NPs generate a bimetallic-like system. Platinum is known for its acidic character and this fact is reflected to its high efficiency catalytic hydrogenation reactions.^[52] Hence, the strong interaction of the basic CNd supports with the Pt NPs, reduces the metal surface acidity.^[53] Consequently, the imprinted Pt NPs on the CNd supports should be more efficient catalysts for oxidation than for reduction reactions.

Catalytic properties

The catalytic properties of the CNd@Pt systems were probed using benzyl alcohol oxidation and cyclohexene hydrogenation as model reactions (Schemes 1 and 2, respectively).



Scheme 1. Oxidation of benzyl alcohol to benzaldehyde.



Scheme 2. Hydrogenation of cyclohexene to cyclohexane.

The oxidation of benzyl alcohol was tested under aerobic conditions in the presence of water without promoters that are usually necessary in these reactions.^[54] Indeed, in the absence of a base, the initial dehydrogenation via H-abstraction is not possible. Alternatively, in the presence of a base, the H is readily abstracted from one of the primary hydroxyl groups and this overcomes the rate limiting step for the oxidation process.^[55] The benzyl alcohol oxidation by CNd@Pt catalysts was highly selective (<99%) for the aldehyde product but presented moderate substrate conversions (14–57% after 4 h, Figure 7a). It is impressive to note the increasing TOF from C0@Pt at 31 h⁻¹ up to 55, 153 and 154 h⁻¹ respectively with the increasing of the N-doping of the support CN0@Pt, CN1@Pt and CN2@Pt (entries 1-4, Table 4).

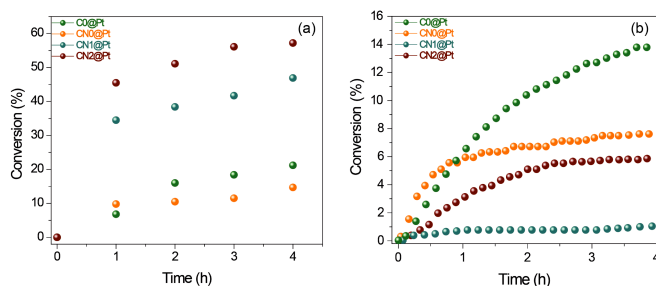


Figure 7. Catalytic performance of the synthesized catalysts CNd@Pt: (a) Benzyl alcohol oxidation and (b) Hydrogenation of cyclohexene.

Table 4. Catalytic properties of CNd@Pt on oxidation and hydrogenation reactions and C0@Pt reference.

| Entry | Catalyst | Substrate | TON | TOF (h ⁻¹) |
|----------------|----------|----------------|-------|------------------------|
| 1 ^a | C0@Pt | Benzyl alcohol | 93 | 31 |
| 2 ^a | CN0@Pt | Benzyl alcohol | 159 | 53 |
| 3 ^a | CN1@Pt | Benzyl alcohol | 459 | 153 |
| 4 ^a | CN2@Pt | Benzyl alcohol | 462 | 154 |
| 5 ^b | C0@Pt | Cyclohexene | 68697 | 22899 |
| 6 ^b | CN0@Pt | Cyclohexene | 8004 | 2668 |
| 7 ^b | CN1@Pt | Cyclohexene | 726 | 242 |
| 8 ^b | CN2@Pt | Cyclohexene | 7263 | 2421 |

Reaction conditions: (a) Oxidation of benzyl alcohol: Pt/benzyl alcohol: 1/500, reaction time: 4 h, deionized water 15 mL, T: 80 °C, P_{O₂}: 4 bar. Products were extracted with toluene and conversion with selectivity determined by GC. (b) Hydrogenation of cyclohexene: Pt/cyclohexene: 1/6360, reaction time: 4 h, T: 25°C, P_{H₂}: 5 bar. Products were extracted with DCM and conversion was determined by GC. (c) TOF = mol products converted/(mol Pt surface × time).^[56]

Therefore, the electron-rich N atoms in the carbon matrix enhance the electronic density over CNd@Pt catalyst (as

observed by XPS) and increase the adsorption rate of benzyl alcohol, promoting a more efficient oxidation reaction, even in the absence of promoters. The same phenomenon is also responsible for the loss of the acidic character by Pt NPs on CNd@Pt catalysts, what is needful to high activity on Pt NPs on hydrogenation reactions.^[52] The hydrogenation of alkenes, such as cyclohexene (Figure 7b), by the CNd@Pt materials display low catalytic activity from 2668 h⁻¹ CN0@Pt, 242 h⁻¹ CN1@Pt and 2421 h⁻¹ CN2@Pt, when compared to orthodox Pt/charcoal as C0@Pt (22899 h⁻¹).^[44] These results indicate that the electronic properties were tuned to high electron density on Pt NPs by CNd supports changing its catalytic properties from reduction to oxidation, clean of co-catalyst or promoters (for oxidation of other alcohols, see Table S7).

Conclusions

N-doped carbon supports play an important role in the overall catalytic process of imprinted naked Pt NPs, hence the support cannot be regarded as a simple mechanical substrate and a phase carrier, but as an important coadjutant in the catalytic process. The effect on the catalytic activity is related to the change of the Pt metallic nature to a richer electron structure when imprinted on the N-doped carbon support. The electronic properties of the imprinted naked Pt NPs are mainly influenced by the nitrogen acid-base behaviour in the N-doped material. The C=N_{pyridinic} sites act as an acid of Lewis, while N_{graphitic} and N_{pyrrolic} sites act as donor ligand-like (Lewis bases) to the Pt NPs. Therefore, the catalytic performance of naked Pt NPs can be modulated by the proper choice of the N-doped carbon supports and by applying a simple donor-acceptor ligand model one can foresee the effect of certain supports on the catalytic and electro-catalytic activities of a system based on naked metallic nanoparticles.

Experimental Section

General

All syntheses were performed using standard Schlenk techniques under an argon atmosphere. CH₃CN and CH₂Cl₂ were purified by standard procedures. The ILs were prepared by previously described procedures^[57]. Elemental analyses were carried out on a CHN Perkin Elmer M CHNS/O Analyser 2400. Raman spectra were acquired on an Olympus spectrometer charge-coupled detector (CCD) and excitation radiation was supplied by a He-Ne laser of 632.8 nm. The N₂ isotherms of the supports, previously degassed at 100 °C under vacuum for 3 h, were obtained using Tristar 3020 Micromeritics equipment. The specific surface areas were determined by the BET multipoint method and the average pore size was obtained by the BJH method. ¹H NMR measurements for the ILs were performed on a Varian 400 MHz. Solid-state ¹³C measurements for the supports were taken using a Varian 500 MHz spectrometer. The infrared spectra were obtained on an ABB FTLA 2000 with a resolution of 4 cm⁻¹. SEM samples were prepared over a metallic support and fixed with carbon tape. SEM images were taken with a Zeiss, LEO EVO 50HV operating at 15 kV. TEM samples were prepared over Cu grid (holey carbon) and dispersed with 2-propanol. TEM images were performed at CMM-UFRGS employing a JEOL-JEM

1200ExII, operating at 100 kV and JEOL-JEM 2010 at 200 kV. XRD were performed using a SIEMENS D500 at IF-UFRGS. XRD diffractograms were taken with a 30 kV current of 25 mA between 20° at 80° (Cu Ka = 1,5418 Å). The Pt depth profiles were determined using RBS with a 1.5 MeV He⁺ incident beam provided by the 3 MV Tandemron accelerator of the IF-UFRGS. XPS measurements were carried out at the LNLS (Brazilian Synchrotron Light Laboratory) at the SXS beam line endstation. The spectra were collected using an InSb (111) double crystal monochromator at fixed photon energy of 1,840 eV. The sample was investigated using the long scan, Pt 4f, N 1s, O 1s and C 1s scan regions. The hemispherical electron analyser (PHOIBOS HSA500 150 R6) was set at a pass energy of 30 eV and the energy step was 0.1 eV, with an acquisition time of 100 ms/point. The monochromator photon energy calibration was done at the Si K edge (1,839 eV). Calibration of the analyser energy was performed using a standard Au (Au 4f_{7/2} peak at 84.0 eV) and using C1s (adventitious carbon, 284.6 eV). The base pressure inside the chamber was around 5 x 10⁻⁹ mbar. CasaXPS was used to fit the XPS results. GC analyses were run with an Agilent Technologies GC System 6820 with a DB-17 column (oven temperature 40°C). GC-MS analyses were run with a Shimadzu QP50 with a Rtx-5MS column (oven temperature 40 °C) employing an ionising voltage of 17 eV.

Synthesis of ILs

The ILs 1-butyl-3-methylimidazolium chloride [BMIm][Cl] and 1-butyl-3-butyl-3-methylimidazolium chloride [BCNMI][Cl] were synthesised using a well described procedure in the literature.^[57] 1,3-Bis(butyl-3-methylimidazolium chloride [DBCNI][Cl]) were synthesised by a mixture of imidazole (68.07 g, 1.0 mol), 1-chlorobutyl-3-methylimidazolium chloride (113.09 g, 1.1 mol) and sodium bicarbonate (84.01 g, 1.0 mol) was dissolved in acetonitrile (150 mL) and stirred under reflux for 24 h. After, the mixture was filtered and to this solution was added 1-chlorobutyl-3-methylimidazolium chloride (113.09 g, 1.1 mol), leaving under stirring and refluxing for 24 h. CH₃CN was evaporated and the product crystallised from a mixture of acetone and methanol. The pure product was obtained in 82.4% yield. By exchanging the chloride anion ILs were prepared by metathesis anion: 1-butyl-3-methylimidazolium dicyanamide [BMIm][dca], 1-butyl-3-methylimidazolium dicyanamide [BCNMI][dca], and of 1,3-bis(butyl-3-methylimidazolium dicyanamide [DBCNI][dca].

1-Butyl-3-methylimidazolium dicyanamide – [BMIm][dca] 1:^[57] ¹H NMR (500 MHz, D₂O, δ): 0.98 (t, J = 7.4 Hz, 3H⁹); 1.35-1.42 (m, 2H⁸); 1.87-1.95 (m, 2H⁷); 3.95 (s, 3H¹⁰); 4.25 (t, J = 7.2 Hz, 2H⁶); 7.51 (d, J = 22.9 Hz, 1H⁵, 1H⁴); 8.76 (s, 1H²). ¹³C RMN (125 MHz, D₂O, δ) 12.67(C⁹); 18.81 (C⁸); 31.30 (C⁷); 35.60 (C¹⁰); 49.29 (C⁶); 119.85 (C¹¹, C¹²); 122.18 (C⁵); 123.45 (C⁴); 135.57 (C²).

1-Butyl-3-methylimidazolium dicyanamide – [BCNMI][dca] 2:^[57] ¹H RMN (500 MHz, D₂O, δ) 2.34 (p, J = 7.0 Hz, 2H⁸); 2.65 (t, J = 7.0 Hz, 2H⁷); 3.96 (s, 3H¹⁰); 4.41 (t, J = 7.0 Hz, 2H⁶); 7.56 (d, J = 29.8 Hz, 1H⁵, 1H⁴); 8.86 (s, 1H²). ¹³C RMN (125 MHz, D₂O, δ) 13.73 (C⁹); 25.08 (C⁷); 35.75 (C¹⁰); 48.01 (C⁶); 119.95 – 119.96 (C¹¹, C¹²); 120.01(C⁹); 122.20 (C⁵); 123.92 (C⁴); 136.26 (C²).

1,3-Bis(butyl-3-methylimidazolium dicyanamide – [DBCNI][dca] 3:^[57] ¹H RMN (500 MHz, D₂O, δ) 2.30 (p, J = 7.0 Hz, 2H⁸, 2H¹²); 2.62 (t, J = 7.0 Hz, 2H⁷, 2H¹¹); 4.39 (t, J = 7.0 Hz, 2H⁶, 2H¹⁰); 7.63 (s, 1H⁴, 1H⁵). ¹³C RMN (126 MHz, D₂O, δ) 13.72 (C⁹, C¹²); 24.94 (C⁷, C¹¹); 48.20 (C⁶, C¹⁰); 119.92 (C⁹, C¹³, C¹⁴, C¹⁵); 122.75 (C⁴, C⁵) 127.66(C²).

General procedure for the synthesis of CNd

Silica template SBA-15 was purchased from Sigma-Aldrich. ILs were infiltrated at 500 mg silica SBA-15 in a large excess under vigorous stirring and reduced pressure until complete infiltration. Any excess of non-infiltrated IL was removed by vacuum filtration. The mass 500 mg of SBA-15 was able to infiltrate nearly the same amount of IL mass. They were then heat treated in an oven at 1000 °C for 1 h under a constant flow of argon^[27]. The black solid obtained was treated with aqueous hydrofluoric acid (HF 4 mol L⁻¹) under stirring until complete dissolution of the silica template. After the material was filtered and washed with deionised water several times, the product was dried by vacuum oven at 100 °C. The samples are referred to by the following designations: **C0** is a Carbon black (30 m².g⁻¹) standard material purchased from Micromeritics and used as reference.^[58] **CN0** for the CNd obtained from the IL 1-butyl-3-methylimidazolium dicyanamide [BMIm][dca], **CN1** for the CNd obtained from the IL 1-butyl-3-methylimidazolium dicyanamide [BCNMI][dca] and **CN2** for the CNd obtained from the IL 1,3-bis(butyl-3-methylimidazolium dicyanamide [DBCNI][dca].

Sputtering deposition of Pt-NPs onto CNd: catalyst preparation

250 mg of CNd were placed within a sample holder arranged horizontally 15 cm from the cathode. After being previously evacuated about 2 μbar, the chamber was filled with argon gas in stable 20 μbar. They were used 40.3 mA voltage 427 V and current in magnetron sputtering technique and subjected to 300 seconds deposition^[59]. After the deposition, the chamber was vented with N₂ and the black powders were recovered and stored under an inert atmosphere for their further characterisation and application. The catalyst is referred according to the CNd source as **CN0@Pt**, **CN1@Pt** and **CN2@Pt**. The same procedure was used to prepare **C0@Pt** from **C0**, Carbon black (30 m².g⁻¹) standard material purchased from Micromeritics and used as reference.

Electrochemical analysis

Work electrodes for cyclic voltammetry were prepared by dispersing the samples (2 mg) in deionised water (2 mL) and 5% of Nafion perfluorinated resin solution (20 μL, Sigma- Aldrich). The mixture was sonicated for 30 min to obtain a homogenous black solution. The obtained solution was drop-cast on a polished gold electrode (2 mm diameter) and was dried in an oven at 30 °C for 20 min. The analysis was performed at room temperature in a three-electrode system. Pt wire was used as a counter electrode. Ag/AgCl were used as a reference electrode for all solutions. Cyclic voltammetry was cycled between -0.2 and 1 V (vs Ag/AgCl) a scan rate 50 mV/s in Ar-saturated solution of H₂SO₄ (0.1 M).

Oxidation of benzylic alcohol

As a general procedure, 15 mL of a solution of benzylic alcohol (BA/Pt = 500) dissolved in water was added to a Fischer-Porter reactor containing the appropriate amount of catalysts. After, the reactor was pressurised with 4 bar of O₂ at 80 °C. Samples were taken from the reaction mixture every 30 min. After the desired reaction time, the reactor was cooled to room temperature and then depressurised. The conversion and selectivity was determined by GC analysis of the reaction samples. The activity values were calculated from the slope of plots of time vs. TON at low substrate conversions: TOF = mol BA converted/(mol Pt surface × time)^[56].

Hydrogenation of cyclohexene

As a general procedure, 1 mL of cyclohexene (CH/Pt = 6360) was added to a Fischer-Porter reactor containing the appropriate amount of catalysts.

After, the reactor was pressurised with 5 bar of H₂ at 25 °C. The reaction was overhauled by consumption of hydrogen through the field logger pressure transducer. The final sample was depressurised and analysed by GC analysis. The activity values were calculated from the slope of plots of time vs. TON at low substrate conversions: TOF = mol CH converted/(mol Pt surface × time)^[56].

Acknowledgements

Thanks, are due to FAPERGS, CNPq and CAPES for financial support. We also would like to thank the CMM/UFRGS and the National Laboratory of Synchrotron Light (LNLS).

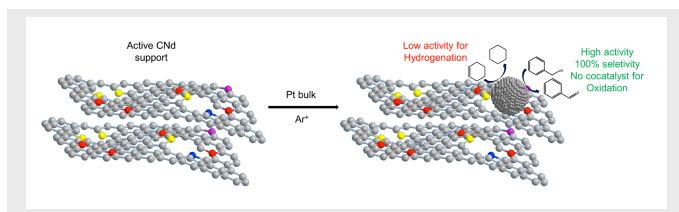
Keywords N-doped carbon, synergistic effect, nanoparticle-support interaction, Platinum nanoparticle, catalysis.

- [1] D. Pantea, H. Darmstadt, S. Kaliaguine, C. Roy, *Appl. Surf. Sci.* **2003**, *217*, 181–193.
- [2] D. Jana, C.-L. Sun, L.-C. Chen, K.-H. Chen, *Prog. Mater. Sci.* **2013**, *58*, 565–635.
- [3] F. B. Su, J. H. Zeng, X. Y. Bao, Y. S. Yu, J. Y. Lee, X. S. Zhao, *Chem. Mater.* **2005**, *17*, 3960–3967.
- [4] Y. Wang, X. Wang, M. Antonietti, *Angew. Chem. Int. Ed.* **2012**, *51*, 68–89.
- [5] X. Zhu, P. C. Hillesheim, S. M. Mahurin, C. Wang, C. Tian, S. Brown, H. Luo, G. M. Veith, K. S. Han, E. W. Hagaman, et al., *ChemSusChem* **2012**, *5*, 1912–1917.
- [6] A. Erto, A. Silvestre-Albero, J. Silvestre-Albero, F. Rodriguez-Reinoso, M. Balsamo, A. Lancia, F. Montagnaro, *J. Colloid Interface Sci.* **2015**, *448*, 41–50.
- [7] Z.-L. Xie, D. S. Su, *Eur. J. Inorg. Chem.* **2015**, *2015*, 1137–1147.
- [8] R. J. White, V. Budarin, R. Luque, J. H. Clark, D. J. Macquarrie, *Chem. Soc. Rev.* **2009**, *38*, 3401–3418.
- [9] E. Lam, J. H. T. Luong, *ACS Catal.* **2014**, *4*, 3393–3410.
- [10] Y. Cao, H. Yu, J. Tan, F. Peng, H. Wang, J. Li, W. Zheng, N. B. Wong, *Carbon N. Y.* **2013**, *57*, 433–442.
- [11] P. Serp, B. Machado, *Nanostructured Carbon Materials for Catalysis*, The Royal Society Of Chemistry, **2015**.
- [12] B. Fang, N. K. Chaudhari, M.-S. Kim, J. H. Kim, J.-S. Yu, *J. Am. Chem. Soc.* **2009**, *131*, 15330–15338.
- [13] B. H. Morrow, A. Striolo, *Nanotechnology* **2008**, *19*, 195711.
- [14] X. X. Wang, Z. H. Tan, M. Zeng, J. N. Wang, *Sci. Rep.* **2014**, *4*, 1–11.
- [15] Y. Shao, J. Sui, G. Yin, Y. Gao, *Appl. Catal. B Environ.* **2008**, *79*, 89–99.
- [16] W. Chen, J. Ji, X. Duan, G. Qian, P. Li, X. Zhou, D. Chen, W. Yuan, *Chem. Commun.* **2014**, *50*, 2142–2144.
- [17] M. C. Gimenez-Lopez, A. Kurtoglu, D. A. Walsh, A. N. Khlobystov, *Adv. Mater.* **2016**, *28*, 9103–9108.
- [18] R. Bussamara, D. Eberhardt, A. F. Feil, P. Migowski, H. Wender, D. P. de Moraes, G. Machado, R. M. Papaléo, S. R. Teixeira, J. Dupont, *Chem. Commun.* **2013**, *49*, 1273–1275.
- [19] H. Wender, R. V. Gonçalves, A. F. Feil, P. Migowski, F. S. Poletto, A. R. Pohlmann, J. Dupont, S. R. Teixeira, *J. Phys. Chem. C* **2011**, *115*, 16362–16367.
- [20] V. Meille, *Appl. Catal. A Gen.* **2006**, *315*, 1–17.
- [21] S. Shrestha, S. Asheghi, J. Timbro, W. E. Mustain, *Appl. Catal. A Gen.* **2013**, *464–465*, 233–242.
- [22] T. Kondo, T. Suzuki, J. Nakamura, *J. Phys. Chem. Lett.* **2011**, *2*, 577–580.
- [23] T. P. Fellinger, A. Thomas, J. Yuan, M. Antonietti, *Adv. Mater.* **2013**, *25*, 5838–5855.
- [24] R. Liu, D. Wu, X. Feng, K. Müllen, *Angew. Chem.* **2010**, *49*, 2565–2569.
- [25] W. Yang, T. P. Fellinger, M. Antonietti, *J. Am. Chem. Soc.* **2011**, *133*, 206–209.
- [26] K. Kwon, Y. J. Sa, J. Y. Cheon, S. H. Joo, *Langmuir* **2012**, *28*, 991–996.
- [27] B. J. P. Paraknowitsch, J. Zhang, D. Su, A. Thomas, M. Antonietti, *Adv. Mater.* **2010**, *22*, 87–92.
- [28] T.-P. Fellinger, D. S. Su, M. Engenhorst, D. Gautam, R. Schlögl, M. Antonietti, *J. Mater. Chem.* **2012**, *22*, 23996.
- [29] R. A. Watile, D. B. Bagal, K. M. Deshmukh, K. P. Dhake, B. M. Bhanage, *J. Mol. Catal. A Chem.* **2011**, *351*, 196–203.
- [30] J. P. Paraknowitsch, A. Thomas, *Macromol. Chem. Phys.* **2012**, *213*, 1132–1145.
- [31] L. Foppa, J. Dupont, C. Scheeren, *RSC Adv.* **2014**, *4*, 16583–16588.
- [32] Y. Qiu, L. Gao, *Chem. Commun.* **2003**, 2378–2379.
- [33] J. P. Paraknowitsch, A. Thomas, M. Antonietti, *J. Mater. Chem.* **2010**, *20*, 6746.
- [34] W. P. Davey, *Phys. Rev. Lett.* **1925**, *25*, 753.
- [35] D.-Q. Yang, G. X. Zhang, E. Sacher, M. José-Yacamán, N. Elizondo, *J. Phys. Chem. B* **2006**, *110*, 8348–8356.
- [36] D.-Q. Yang, E. Sacher, *Chem. Mater.* **2006**, *18*, 1811–1816.
- [37] G. Zhang, D. Yang, E. Sacher, *J. Phys. Chem. C* **2007**, *111*, 565–570.
- [38] G. He, Y. Song, K. Liu, A. Walter, S. Chen, S. Chen, *ACS Catal.* **2013**, *3*, 831–838.
- [39] F. Su, Z. Tian, C. K. Poh, Z. Wang, S. H. Lim, Z. Liu, J. Lin, *Chem. Mater.* **2010**, *22*, 832–839.
- [40] M. P. Languer, F. R. Scheffer, A. F. Feil, D. L. Baptista, P. Migowski, G. J. Machado, R. Teixeira, D. E. Weibel, *Int. J. Hydrogen Energy* **2013**, *38*, 14440–14450.
- [41] V. S. Souza, J. D. Scholten, D. E. Weibel, D. Eberhardt, D. L. Baptista, S. R. Teixeira, J. Dupont, *J. Mater. Chem. A* **2016**, *4*, 7469–7475.
- [42] J. Robertson, C. A. Davis, *Diam. Relat. Mater.* **1995**, *4*, 441–444.
- [43] Z. Hamoudi, E. A. M. Khakani, M. Mohamedi, *Electroanalysis* **2011**, *23*, 1205–1211.
- [44] L. Perini, C. Durante, M. Favaro, V. Perazzolo, S. Agnoli, O. Schneider, G. Granozzi, A. Gennaro, *ACS Appl. Mater. Interfaces* **2015**, *7*, 1170–1179.
- [45] W. Chen, J. T. Muckerman, E. Fujita, *Chem. Commun.* **2013**, *49*, 8896–8909.
- [46] W. Chen, S. Iyer, S. Iyer, K. Sasaki, C.-H. Wang, Y. Zhu, J. T. Muckerman, E. Fujita, *Energy Environ. Sci.* **2013**, *6*, 1818–1826.
- [47] O. L. Li, S. Chiba, Y. Wada, H. Lee, T. Ishizaki, *RSC Adv.* **2016**, *6*, 109354–109360.

- [48] H. Zhang, Z. Ma, J. Duan, H. Liu, G. Liu, T. Wang, K. Chang, M. Li, L. Shi, X. Meng, et al., *ACS Nano* **2016**, *10*, 684–694.
- [49] J. Tymoczko, F. Calle-vallejo, W. Schuhmann, A. S. Bandarenka, *Nat. Commun.* **2016**, *7*, 1–6.
- [50] M. Shao, P. Liu, J. Zhang, R. Adzic, *J. Phys. Chem. B* **2007**, *111*, 6772–6775.
- [51] D. S. Su, S. Perathoner, G. Centi, *Chem. Rev.* **2016**, *113*, 5782–5816.
- [52] C. W. Scheeren, G. Machado, J. Dupont, P. F. P. Fichtner, S. R. Teixeira, *Inorg. Chem.* **2003**, *42*, 4738–4742.
- [53] G. Centi, S. Perathoner, D. S. Su, *Catal. Surv. Asia* **2014**, *18*, 149–163.
- [54] C. Mondelli, J.-D. Grunwaldt, D. Ferri, A. Baiker, *Phys. Chem. Chem. Phys.* **2010**, *12*, 5307–5316.
- [55] T. Mallat, A. Baiker, *Chem. Rev.* **2004**, *104*, 3037–3058.
- [56] A. P. Umpierre, E. de Jesús, J. Dupont, *ChemCatChem* **2011**, *3*, 1413–1418.
- [57] H. Srour, H. H. Rouault, C. C. Santini, Y. Chauvin, *Green Chem.* **2013**, *15*, 1341–1347.
- [58] M. Ali, G. Abarca, D. Eberhardt, A. Gual, F. Bernardi, S. R. Teixeira, J. Dupont, *Tetrahedron* **2017**, *73*, 5593–5598.
- [59] A. Kauling, G. Ebeling, J. Morais, A. Pádua, T. Grehl, H. H. Brongersma, J. Dupont, *Langmuir* **2013**, *29*, 14301–14306.

Layout 2:

FULL PAPER



A synergic effect between small and well distributed Pt nanoparticles (NPs) and N-doped carbons naked Pt nanoparticles accounts for the electronic structure of resulting materials. Naked Pt nanoparticles obtained by sputtering deposition onto N-doped carbons display high electro (catalytic) activity for oxidation reactions and poor activity for hydrogenation reactions. The simple donor-acceptor metal-ligand model can be used for the design of supported metal NPs on carbon supports with controlled electronic properties.

Gustavo R. Bolzan,^[a] Gabriel Abarca,^[a]
Wellington D. G. Gonçalves,^[a] Carolina
F. Matos,^[b] Marcos J. L. Santos^[a] and
Jairton Dupont^{*[a]}

Page No. – Page No.

Imprinted naked Pt nanoparticles on N-doped carbon supports: A synergistic effect between catalyst and support